energies

MDPI

Article

Optimizing the Performance of Solo Duck Wave Energy Converter in Tide

Jinming Wu [1], Yingxue Yao [2,*], Wei Li [3], Liang Zhou [1] and Malin Göteman [3]

[1] Department of Mechanical Engineering, Harbin Institute of Technology, Harbin 150001, Heilongjiang, China; wujinming@hit.edu.cn (J.W.); lzhou@hit.edu.cn (L.Z.)
[2] Shenzhen Graduate School, Harbin Institute of Technology, Shenzhen 518055, Guangdong, China
[3] Department of Engineering Science, Uppsala University, Uppsala 75121, Sweden; wei.li@angstrom.uu.se (W.L.); malin.goteman@angstrom.uu.se (M.G.)
* Correspondence: yxyao@hit.edu.cn; Tel.: +86-755-2603-6868

Academic Editor: Stephen Nash
Received: 24 January 2017; Accepted: 22 February 2017; Published: 28 February 2017

Abstract: The high efficiency performance of the Edinburgh Duck wave energy converter (WEC) in 2D regular wave tests makes it a promising wave energy conversion scheme. A solo Duck WEC will be able to apply the point absorber effect to further enhance its performance. Since released degree of freedom will decrease the efficiency, a Duck WEC with fixed pitching axis will be a better option. However, for fixed supported WECs, tide is a non-ignorable consideration. In this paper, a movable mass method is utilized in the whole tidal range to not only balance the Duck to appropriate beak angles, but also follow the variation of hydrodynamic coefficients to keep cancelling the reactance of the system impedance so that complex conjugate control can be realized to optimize the power capture performance of the Duck WEC in tide. Results show that the beak angle should be adjusted to as large a value as possible so that the response amplitude of the Duck at maximum relative capture width will be reasonable small, and the lowest weight of the movable mass is found when its designed position locates at the center of the Duck profile.

Keywords: solo Duck; hydrodynamic coefficients; complex conjugate control; maximum relative capture width; movable mass method

1. Introduction

In order to develop a cleaner and safer energy supply, ocean wave energy conversion has been attracting extensive research in recent years [1–3]. The Edinburgh Duck wave energy converter (WEC), which was invented by Stephen Salter in 1974 [4], is one of the most efficient wave energy conversion schemes ever proposed. The Duck WEC is of terminator type, and one proposal of its cross section is shown in Figure 1a [5]. The cross section rotates about O and its profile can be divided into three parts: stern, paunch and beak. The stern part is of circular shape with O as its center point. The paunch part is formed so that the profile matches the diameter of the orbital movement of water particles at each depth [6]. The high efficiency character of this cross section results from its asymmetrical property. Evans [7] and Mei [8] had revealed that, for a two-dimensional cylinder with single pitching mode, the maximum efficiency $E_{\max}$ can be calculated by:

$$E_{\max} = \frac{1}{1 + |A^- / A^+|^2} \tag{1}$$

where A^+ and A^- are the radiated wave amplitude at $x \to +\infty$ and $x \to -\infty$ due to forced unit amplitude pitching velocity. Since the circular stern part of the Duck produces only very small

wave amplitude leeward, the maximum efficiency will be high. Experimental tests in regular wave conditions confirmed more than 90% efficiency [9] and validated this theory.

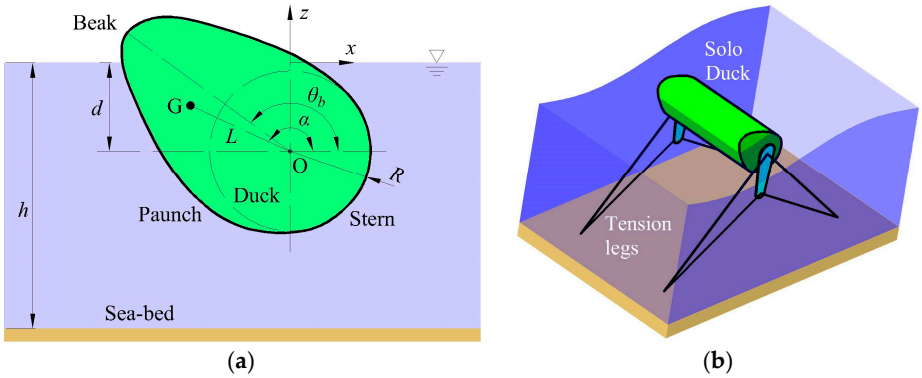

Figure 1. Geometry of the solo Duck wave energy conversion (WEC): (**a**) plane view of the Duck cross section; and (**b**) isometric view of the taut mooring configuration for a Duck with fixed pitching axis in head on waves.

In the early design envisage of the Duck WEC, a plurality of Duck members are connected by end to end jointed spines with the intention to average the hydrodynamic forces on the axis supporting system so that the mooring forces are reduced in real sea wave climate [6]. However, the mechanical system was very complex, and the estimated low reliability of the system, especially the high failure rate of the mooring cables, caused the UK government to cancel the project [9]. Later, the research interest of the Duck WEC has shifted to the solo Duck configuration, whose efficiency will be further increased by applying the point absorber effect [5,10] and the mooring system may also be simpler. Skyner applied a sophisticated supporting rig to measure the hydrodynamic coefficients of a solo Duck, based on which the power absorption was predicted and agreed well with experimental results, and it showed that the solo Duck can achieve a capture width 1.6 times the Duck width in regular wave, and the theoretical maximum capture width can be achieved by applying a complex conjugate controller by setting the controller impedance as the complex conjugate of the radiation impedance [5]. Pizer used a three-dimensional linear wave diffraction program to investigate the performance of a solo Duck, and motion constraints are also studied when taking both physical and linear theory limitations into consideration, and results revealed that although under constraints the solo Duck can achieve a relative capture width of over 2 and the performance decreases with more released motion freedom [10]. Actually, this performance reducing character is also observed in the spine based Duck investigated by Mynett et al. [11]. Thus, for a solo Duck WEC, a fixed pitching axis is a better option. One possible taut mooring configuration for the Duck with fixed pitching axis in head on waves is shown in Figure 1b. This mooring scheme is evolved from the multi-degree-of-freedom-power-absorbing mooring configuration proposed in [10] by removing the power take-off (PTO) devices from the tension legs. If the margin of the pre-tension and the stiffness of the tension legs are large enough, we can treat the Duck pitching axis as fixed. For a fixed supporting WEC, tide is a non-ignorable consideration. Castellucci et al. [12–14] investigated the effect of tide to the performance of wave energy converters, and proposed a tide compensation method to reduce the influence of tide by expanding and contracting the length of the connection line for a fixed stator point absorber WEC. In a tidal period, the fixed pitching axis Duck is exposed to continuously varying tidal height, resulting in its varying floating states in equilibrium position. The corresponding hydrodynamic coefficients and hydrostatic stiffness coefficients will also change accordingly, causing the Duck to deviate from its designed optimal working state.

In order to optimize the performance of a wave energy sea water desalination device at different wave climate, Lucas et al. [15] used the removable mass method by realizing complex conjugate control.

However, the best designed position of the movable mass is not investigated. In this paper, the movable mass method is utilized in the whole tidal range to not only balance the Duck to appropriate beak angles in different tidal heights, but also follow the variation of hydrodynamic coefficients to keep cancelling the reactance of the system impedance so that complex conjugate control can be realized to optimize power capture performance of the Duck WEC in tide. At first, the character of hydrodynamic coefficients is studied for a range of floating states at different tidal heights. Then, the maximum relative capture width achieved by applying complex conjugate control at different floating states is investigated to determine the best floating state at different tidal heights. Furthermore, the hydrostatic stiffness coefficient is studied to confirm the feasibility of realizing the optimal control by adjusting the position of the mass center. Finally, a case study is performed based on the previous results to find the trajectory of the movable mass in tide and to find the best designed position of the movable mass to achieve the lowest movable mass weight.

2. Geometry and Floating States of the Duck

The detailed description of the geometry of the solo Duck is shown in Figure 1, where θ_b is the beak angle; d is the depth of rotation axis O, i.e., the pitching axis; R is the radius of the stern part; G is the gravity center of the rotating mass; L and α are the radial distance and angle of the gravity center of the rotating mass, respectively; and h is the water depth. Oxyz is the global Cartesian coordinate system with x in wave propagating direction, y in longitudinal direction of the Duck and z in the opposite direction of gravity with $z = 0$ representing the still water level. The dimension of the Duck is the same as that in [10] and is 100:1 scale compared to the dimension of the experimental model used in [5]. In accordance with the experimental setup, we have $h = 60$ m, $R = 5$ m and the width of Duck $W = 29$ m.

At different tidal heights, the Duck will present different floating states. In order to understand the influence of tidal height on the hydrodynamic performance of the Duck, a range of floating states are studied. Although the tidal range differs globally, the overall law is that the nearer the coast, the larger the tidal range [16,17]. Since the solo Duck WEC is an off-shore device in open sea, we choose the tidal range to be $H_T = 3$ m, which belongs to the meso-tidal range (2–4 m) [18]. The floating state of the Duck is characterized by two parameters: the depth of rotation axis d and the beak angle θ_b, and their values are listed in Table 1. Floating states No. 1–5 vary the depth of rotation axis from the lowest tidal height $-H_T/2$ to the highest $H_T/2$ with the beak angle be kept constant at $\theta_b = 132^\circ$. Floating states No. 6–9 vary the beak angle from 108°, where the Duck almost loses its asymmetry property, to 156°, where the beak nearly touches the free surface, with the depth of rotation axis be kept constant at $d = 5.5$ m. Therefore, the listed floating states represent a large range of attitudes the Duck is possible to present in different tidal heights.

Table 1. Value of characteristic parameters of the floating state.

Floating State No.	1	2	3	4	5	6	7	8	9
d, m	4	4.75	5.5	6.25	7	5.5	5.5	5.5	5.5
θ_b, deg	132	132	132	132	132	108	120	144	156

3. Theoretical Modeling

In this paper, the linear wave theory is applied to study the hydrodynamic performance of the solo Duck at different floating states. Assume the wave amplitude to be small relative to the wavelength, and the water particle motion to be irrotational and incompressible. Complex amplitudes are used to simplify the expressions. Pitch excursion of the Duck WEC is defined as:

$$\xi = \mathrm{Re}\left\{\hat{\xi} e^{i\omega t}\right\} \tag{2}$$

where $\hat{\xi}$ is the complex amplitude of pitch excursion; ω is the circular frequency of incident wave; and t is the flow time. Hence, the complex amplitude of pitch velocity can be obtained as:

$$\dot{\hat{\xi}} = i\omega\hat{\xi} \tag{3}$$

and the complex amplitude of pitch acceleration as:

$$\ddot{\hat{\xi}} = -\omega^2\hat{\xi} \tag{4}$$

We can easily get the dynamic motion equation of the Duck as:

$$[-(J + J_e)\omega^2 + (C + C_e)i\omega + K_r]\hat{\xi} = \hat{M} \tag{5}$$

where J, C and K_r are the added inertia, radiation damping coefficient and hydrostatic stiffness coefficient of the Duck in pitch direction due to pitch motion, respectively; J_e is the dry inertia of the Duck itself in pitch direction; C_e is the PTO damping coefficient; and $\hat{M}$ is the complex amplitude of excitation moment in pitch direction. In accordance with the definition in [19], we define the system impedance as the summation of the radiation impedance and mechanical impedance by:

$$Z_s = \omega(C + C_e) + [K_r - \omega^2(J + J_e)]i \tag{6}$$

where $\omega(C + C_e)$ is the resistance term and $[K_r - \omega^2(J + J_e)]i$ is the reactance term. The complex amplitude of wave amplitude $\hat{A}$ is defined as:

$$\hat{A} = A_0 \tag{7}$$

where A_0 is the amplitude of incident wave and it is a real value. Then, the complex amplitude of pitch excursion can be expressed by:

$$\hat{\xi} = A_0\xi_0 e^{i\Phi} \tag{8}$$

where ξ_0 is the modulus of complex amplitude of pitch excursion per unit wave amplitude; and ϕ is phase difference between the complex amplitude of pitch excursion and $\hat{A}$. In addition, the excitation moment can be expressed by:

$$\hat{M} = A_0 M_0 e^{i(\Phi+\Psi)} \tag{9}$$

where M_0 is the modulus of complex amplitude of excitation moment per unit wave amplitude; and ψ is phase difference between the complex amplitude of excitation moment and $\hat{\xi}$. By inserting the expression for $\hat{\xi}$, $\hat{M}$ and Z_s into Equation (5), the pitch excursion per unit wave amplitude is obtained as:

$$\xi_0 = \frac{M_0}{Z_s} e^{i\Psi} \tag{10}$$

The power captured by the Duck can be calculated by:

$$P_{capture} = \frac{1}{2} C_e \dot{\hat{\xi}} \dot{\hat{\xi}}^* = \frac{1}{2} C_e \omega^2 A_0^2 \xi_0^2 = \frac{C_e \omega^2 A_0^2 M_0^2}{2|Z_s|^2} \tag{11}$$

where * denotes the complex conjugate. In linear regular wave, for finite water depth, the incident wave power flux per unit wave front can be calculated by [20,21]:

$$P_{incident} = \frac{\rho g A_0^2 \omega}{4k}\left[1 + \frac{2kh}{\sinh(2kh)}\right] \tag{12}$$

where ρ is the density of water, g is the acceleration of gravity, k is the wave number, and they satisfy the dispersion relation:

$$\omega^2 = gk\tan(kh) \tag{13}$$

The relative capture width η, which is extensively used in representing the efficiency of WECs [22–24], is defined by dividing the captured power by incident power flux and characteristic length of the WEC. For the solo Duck, the relative capture width becomes:

$$\eta = \frac{P_{capture}}{P_{incident}W} = \frac{2M_0^2\omega^3 C_e}{\rho g^2 W|Z_s|^2}\frac{1}{\tanh(kh)\left[1+\frac{2kh}{\sinh(2kh)}\right]} \tag{14}$$

In Equation (14), the added inertia, damping coefficient and excitation moment are calculated by the boundary element method (BEM) by using ANSYS AQWA [25] software (Version 16.0; ANSYS: Canonsburg, PA, USA). Since the Duck is symmetrical to the y = 0 plane, only half of the Duck is modeled to decrease computational costs. Figure 2 shows an example of the BEM mesh for the Duck at floating state No. 8. A total of 1250 panels are used to model the Duck surface. However, only diffraction panels under the free surface will be computed, while the panels above the free surface are neglected.

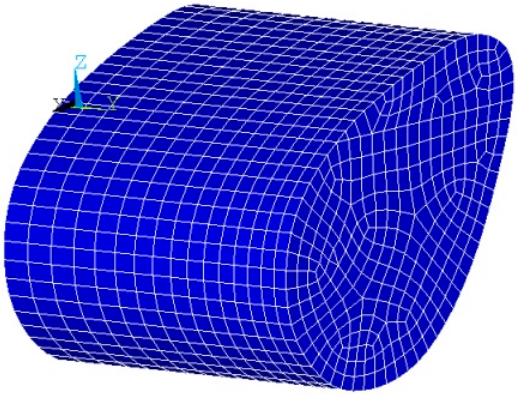

Figure 2. An example of the boundary element method (BEM) mesh for the Duck at floating state No. 8.

The BEM method is validated by comparing the calculated hydrodynamic coefficients with the experimental results in [5]. The floating state of the Duck in the experiment is the same as the floating state No. 8 but with a 1:100 scale of dimension. Thus, the floating state No. 8 is scaled to the same dimension of the experimental setup and the water density is set to 1000 kg/m^3 to keep consistent with the fresh water used in the wave tank. The comparison results are shown in Figure 3, where Z, which is called "radiation impedance" in [5], is defined as:

$$Z(\omega) = C(\omega) + i\omega J(\omega) + i\omega J_e + \frac{1}{i\omega}K_r \tag{15}$$

In the experimental setup, J_e = 0.0636 Kg·m^2, and K_r = 1.165 N·m. The BEM results agree well the experiment indicating that the BEM method is credible to predict the hydrodynamic coefficients of the solo Duck at other floating states.

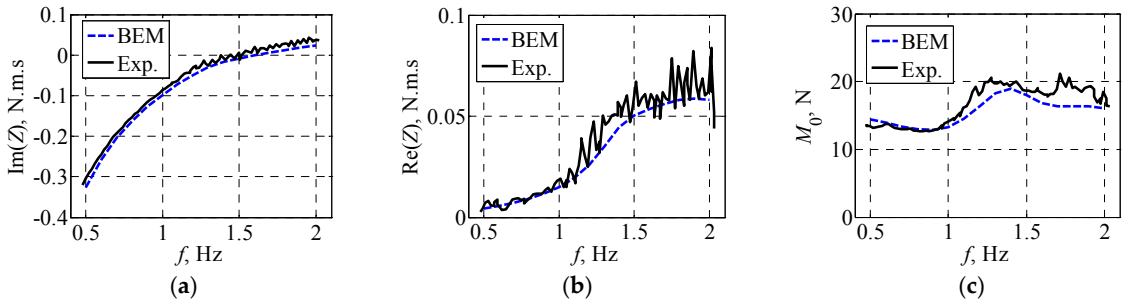

Figure 3. Comparison of hydrodynamic coefficients between the BEM and experimental results for 1:100 scaled Duck at floating state No. 8: (**a**) added inertia; (**b**) radiation damping coefficient; and (**c**) excitation moment coefficient.

4. Results and Discussion

In this section, the character of hydrodynamic coefficients is firstly studied for a range of floating states at different tidal heights. Then, the maximum relative capture width achieved by applying complex conjugate control at different floating states is investigated to determine the best floating state at different tidal heights. Furthermore, the hydrostatic stiffness coefficient is studied to confirm the feasibility of realizing the optimal control by adjusting the position of the mass center. Finally, a case study is performed based on the previous results to find the trajectory of the movable mass in tide and to find the best designed position of the movable mass to achieve the lowest movable mass weight.

4.1. Hydrodynamic Coefficients

Figure 4 shows the added inertia as a function of wave frequency at different floating states. The added inertia increases with depth of rotation axis monotonously when $\theta_b = 144^\circ$ and also increases with beak angle monotonously when $d = 5.5$ m. From Salter's experimental result, one conclusion is made that the added inertia of the Duck increases with water line length [26]. Figure 5 shows the added inertia variation with characteristic parameters of the wetted surface of the Duck at different wave frequencies. In Figure 5a, we find that the added inertia increases with water line length only when the depth of rotation axis is fixed, while this relation is reversed when the beak angle is fixed. In general, the added inertia varies disorderly with the water line length. In fact, the added inertia is physically caused by the synchronous motion of the water near the oscillating body surface. In Figure 6a, a small piece of water near the wetted surface of the Duck is shown to demonstrate its flow pattern. Suppose the surface of the Duck is impermeable and of non-slip condition, which is the common case, the water particles at the wetted surface will follow its motion velocity. Then, the water near the wetted surface will follow the oscillating pitch motion of the Duck. Although the flow pattern is essentially very complex, we believe that the volume of the followed water should be proportional to the width of the water piece, which is the mapped length of the small segment on the Duck surface in the normal direction of its velocity. In addition, according to the definition of moment of inertia, the inertia of the followed water should also be proportional to square of its rotating radius. Here, we define a new parameter, named water inertia, to include all relevant parameters that are proportional to water inertia to account for the added inertia caused by the followed water oscillation as:

$$J_w = ds \cdot \cos\gamma \cdot l^2 \tag{16}$$

where ds is the length of the segment on the Duck surface; γ is the angle between the normal vector of the segment and its velocity direction; and l is the rotation radius. Hence the water inertia will be proportional to added inertia. Figure 6b shows the distribution of the water inertia over the wetted surface of the Duck at $d = 5.5$ m and $\theta_b = 144^\circ$. The paunch part contributes most to the water inertia, while the contribution from the stern part is small. Especially in the circular stern part, the water inertia

is almost zero. The total water inertia for the Duck at certain floating state is obtained by integrating Equation (16) over the whole wetted surface. Figure 5b shows the added inertia variation with the total water inertia at different wave frequencies. It is interesting to find that the distribution of the added inertia is almost reduced to a straight line, which agrees with the previous hypothesis that the water inertia be proportional with added inertia. The fitted lines for different wave frequencies are also shown in Figure 5b. Small scattering of the points from the fitted lines are observed indicating that the added inertia caused by the oscillation water motion is very complex and more elaborate calculation should be performed to precisely predict the added inertia. However, we found that the total water inertia is an important factor to qualitatively estimate the added inertia of Duck at certain wave frequency, and this provides a profile reference parameter in understanding the added inertia and even designing the profile of other pitching devices without performing large amount of BEM simulations ahead.

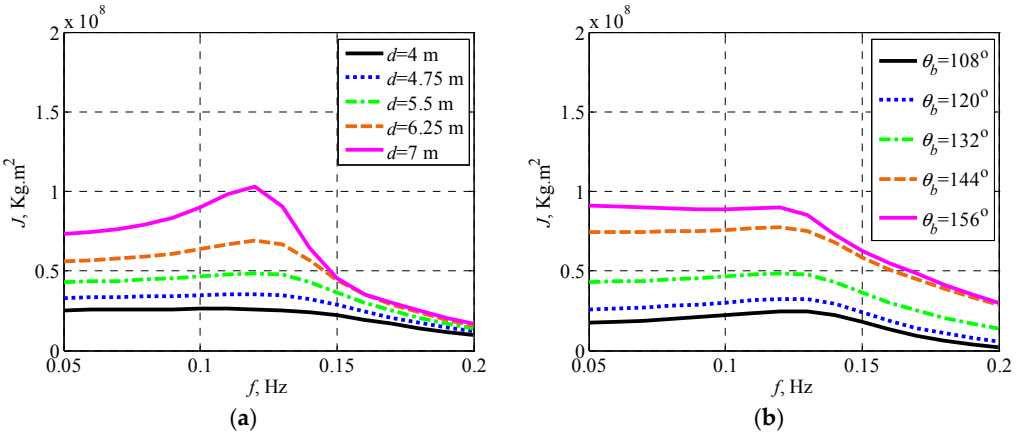

Figure 4. Added inertia as a function of wave frequency at different floating states: (**a**) for fixed beak angle at θ_b = 144°; and (**b**) for fixed depth of rotation axis at d = 5.5 m.

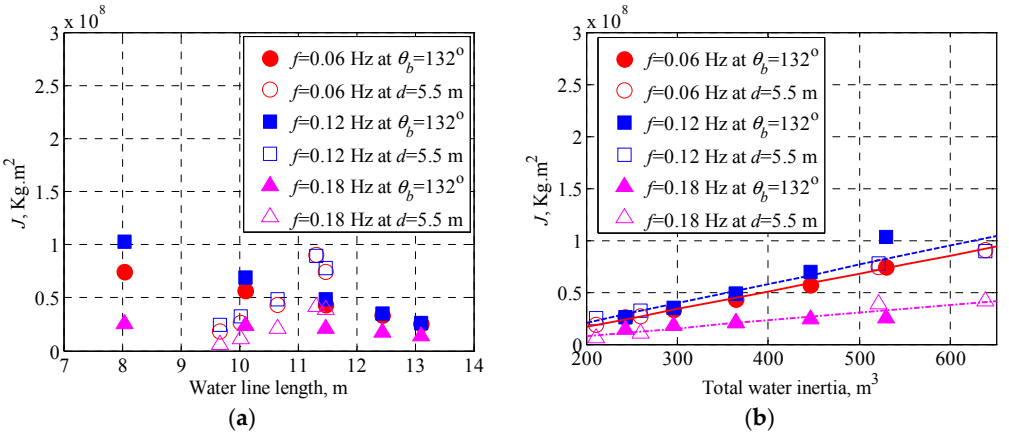

Figure 5. Added inertia variation with characteristic parameters of the wetted surface of the Duck at different wave frequencies: (**a**) for water line length; and (**b**) for total water inertia. The red solid line, blue dashed line and magenta dash-dot line denote the fitted lines at f = 0.06, 0.1 and 0.16 Hz, respectively.

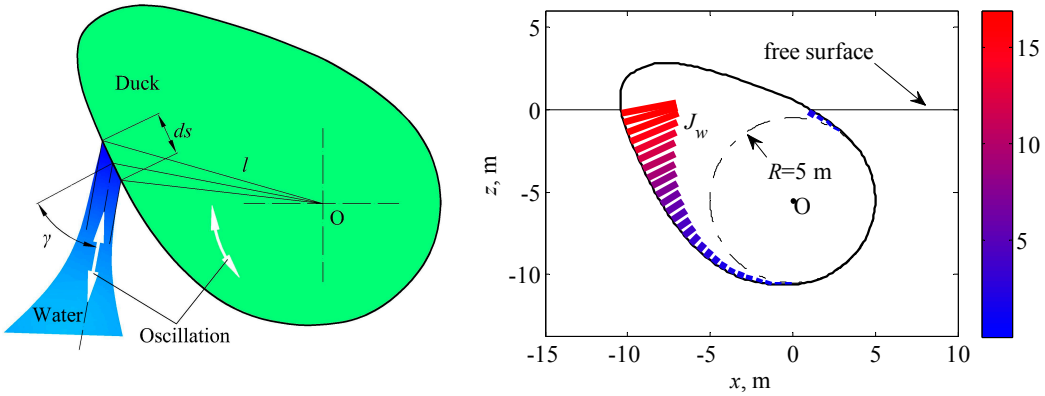

(**a**) (**b**)

Figure 6. Demonstration of the water inertia: (**a**) the flow pattern of a small piece of water near the wetted Duck surface; and (**b**) distribution of the water inertia along the wetted Duck surface at d = 5.5 m and $\theta_b = 144°$.

Figure 7 shows the radiation damping coefficient as a function of wave frequency at different floating states. The radiation damping coefficient increases with beak angle monotonously when $\theta_b = 144°$ and also increases with beak angle when d = 5.5 m and a little exception is observed for beak angle of 156° at frequencies around 0.2 Hz, where the radiation damping coefficient decreases with beak angle. Figure 8 shows the excitation moment coefficient as a function of wave frequency at different floating states. The excitation moment coefficient increases with depth of rotation axis when $\theta_b = 144°$ and increases with beak angle when d = 5.5 m, and a small decreasing trend is observed for the beak angle of 156° at frequencies around 0.2 Hz. Actually, the similar variation law of the added inertia, radiation damping coefficient and excitation moment coefficient with floating states is expected, since they all only depend on the shape of the wetted surface at certain frequency. The same variation in the wetted surface shape may be reasonable to result in the same variation in hydrodynamic coefficients.

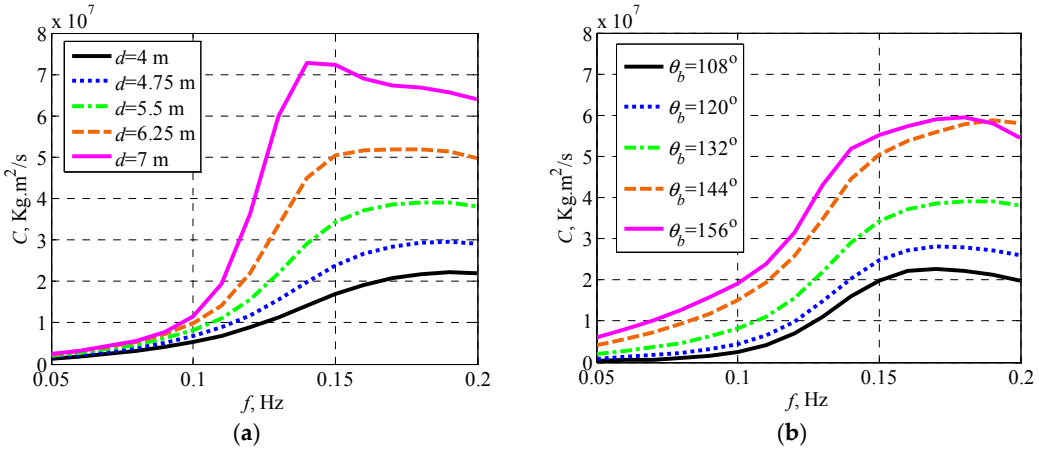

(**a**) (**b**)

Figure 7. Radiation damping coefficient as a function of wave frequency at different floating states: (**a**) for fixed beak angle at $\theta_b = 144°$; and (**b**) for fixed depth of rotation axis at d = 5.5 m.

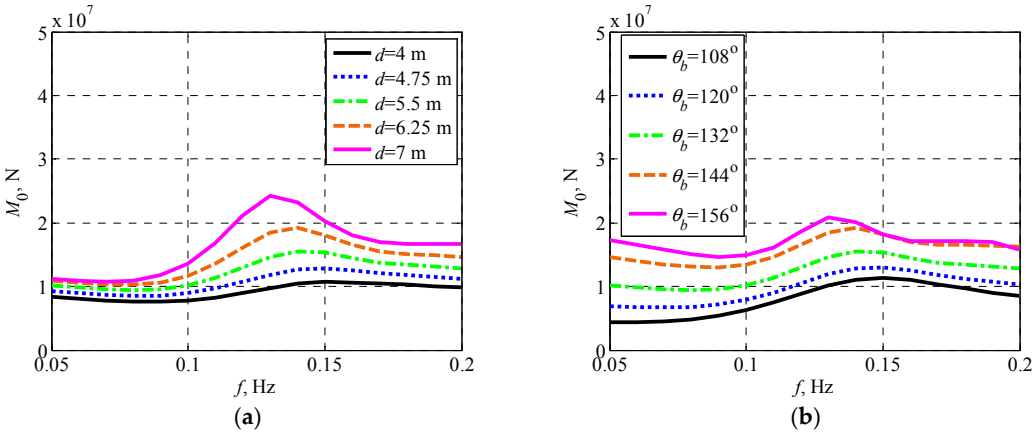

Figure 8. Excitation moment coefficient as a function of wave frequency at different floating states: (**a**) for fixed beak angle at θ_b = 144°; and (**b**) for fixed depth of rotation axis at d = 5.5 m.

4.2. Maximum Relative Capture Width

According to Equation (14), the maximum relative capture width of the solo Duck WEC is obtained when:

$$K_r = (J + J_e)\omega^2 \tag{17}$$

and:

$$C_e = C \tag{18}$$

That means the Duck WEC works at resonance and the PTO damping is optimal, i.e., the Duck is under the phase and amplitude control, also called complex conjugate control [19]. Then, the maximum relative capture width is obtained as:

$$\eta_{\max} = \frac{M_0^2\omega}{2\rho g^2 WC}\frac{1}{\tanh(kh)\left[1+\frac{2kh}{\sinh(2kh)}\right]} \tag{19}$$

As shown in Equation (19), when neglecting the second fraction of the right term representing the influence of water depth, the maximum relative capture width at certain frequency is determined only by excitation moment and radiation damping coefficient, but not by the added inertia. In addition, the reader may find that M_0, which represents the diffracting term, in Equation (19) does not appear in Equation (1), which is also an expression for the maximum efficiency and only radiation terms are included. Actually, the two equations are consistent as both of them have two arguments that are directly related to the geometry of the Duck. More thoroughly, the radiation term can be related to the diffracting term [27] by:

$$C = \frac{1}{8\lambda P_{incident}}\int_0^{2\pi} M_0{}^*(\theta)M_0(\theta)\mathrm{d}\theta \tag{20}$$

where λ is the wavelength of incident wave; and θ is the direction angle of the incident wave. Therefore, M_0 and C are just the synthetic reflection of A^+ and A^-, and Equations (1) and (19) should present the same results.

Figure 9 shows the maximum relative capture width as a function of wave frequency at different floating states. For both subfigures, an overall decreasing trend of the maximum relative capture width with frequency is observed. Small rise and fall of the maximum relative capture width in the frequency range and the resulted local maxima and minima are also detected. The larger the depth of rotation axis and beak angle, the more prominent the fluctuation amplitudes appears. For most of the wave frequencies studied in this paper, the maximum relative capture width exceeds one, which is the limitation for a spine based Duck WEC and its hydrodynamic performance is dominated

by the 2D property. This indicates that the solo Duck WEC effectively uses the point absorber effect to improve its power capture ability. Therefore, the solo Duck WEC will have better efficiency advantage than its spine based counterpart. Another interesting finding is that the maximum relative capture tends to converge at small wave frequency. This may be due to that the attitude differences between these floating states are relatively small compared to the large wavelength at low frequencies.

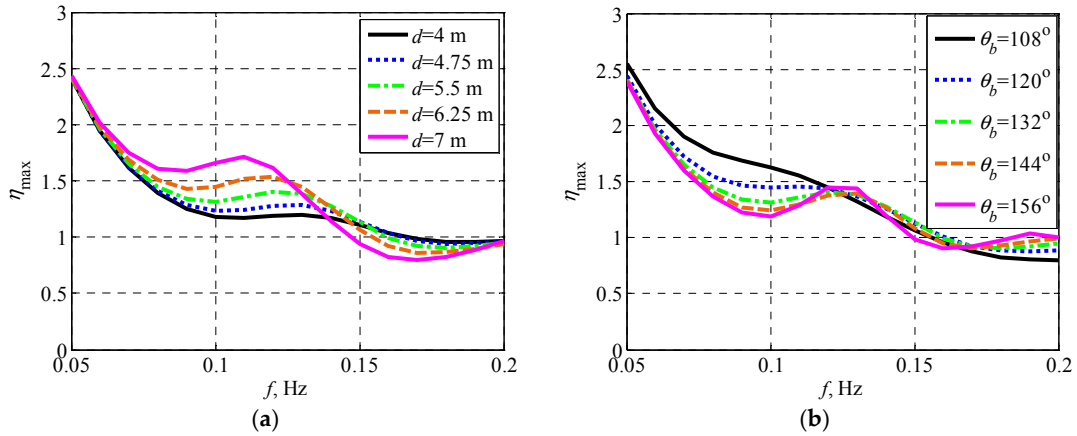

Figure 9. Maximum relative capture width as a function of wave frequency at different floating states: (**a**) for fixed beak angle at $\theta_b = 144^\circ$; and (**b**) for fixed depth of rotation axis at $d = 5.5$ m.

In Figure 9, the maximum relative capture width is achieved by applying the complex conjugate control. However, several studies [28–30] have revealed that it should be careful that a complex conjugate control applied to a point absorber in long waves may result in large motion excursion, which may be unsuitable due to both physical and linear wave theory limitations. The response amplitude operator (RAO) of the solo Duck at the maximum relative capture width can be determined from Equations (10), (17) and (18) as:

$$\xi_{0\max} = \frac{M_0}{2\omega C} \tag{21}$$

Figure 10 shows the RAO of the Duck at maximum relative capture width as a function of wave frequency at different floating states. The RAO decreases with wave frequency monotonously in the whole frequency range, and it is more sensitive to the variation of beak angle than that of depth of rotation axis. In long waves, the RAO is quite large. However, the RAO decreased a lot when the beak angle increases. This inspired us that in order to make the complex conjugate control more credible and feasible, the beak angle should be adjusted to as large value as possible. When considering the optimal floating state in tide, we decide that the beak angle should be adjusted large enough until only 2 m freeboard height left above the free surface at every tidal height. The resulting beak angles in different tidal heights corresponding to different rotation axis depths are listed in Table 2, where d_T is the tidal height.

Table 2. Value of beak angle at different tidal heights.

d_T, m	−1.5	−0.75	0	0.75	1.5
d, m	4	4.75	5.5	6.25	7
θ_b, deg	162.0	155.4	150.3	144.9	139.2

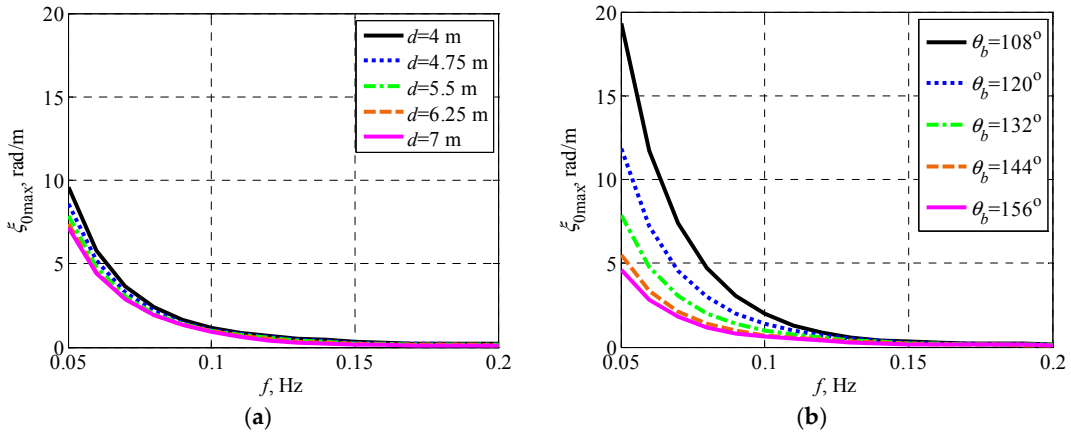

Figure 10. Response amplitude operator (RAO) of the Duck at maximum relative capture width as a function of wave frequency at different floating states: (**a**) for fixed beak angle at $\theta_b = 144°$; and (**b**) for fixed depth of rotation axis at $d = 5.5$ m.

4.3. Hydrostatic Stiffness Coefficient

The hydrostatic stiffness coefficient of the Duck also depends on the floating state, and it can be divided into two parts: the pressure moment coefficient K_P and the gravity moment coefficient K_G. The pressure moment of the Duck applied by the water at the rotation axis can be calculated by:

$$M_P = \rho g \iint_{S_b} z\boldsymbol{n} \times \boldsymbol{r} \mathrm{d}S \tag{22}$$

where S_b is the wetted surface; $\boldsymbol{n}$ is the outward normal vector on the wetted surface; and $\boldsymbol{r}$ is the vector from the point on the wetted surface to the rotation axis O. The pressure moment coefficient can be calculated as [31]:

$$K_P = \rho g \iint_{S_b} x^2 n_3 \mathrm{d}S + \rho g v (z_b + d) \tag{23}$$

where n_3 is the z-component of the normal vector $\boldsymbol{n}$; z_b is the z-component coordinate of buoyancy center; and v is the volume of water displaced by the Duck. Figure 11 shows the pressure moment and pressure moment coefficient as a function of depth of rotation axis and beak angle. The pressure moment increases with both depth of rotation axis and beak angle. An intuitional explanation is that the submerged volume increases with depth of rotation axis and beak angle, and then resulted in the buoyancy and buoyancy moment increasing. Actually, the pressure moment coefficient can be deduced from the pressure moment from its definition by:

$$K_P = \frac{\mathrm{d}M_P}{\mathrm{d}\theta_b} \tag{24}$$

From Figure 11a, it can be seen that in both sides of the pressure moment $M_P = 0.9 \times 10^8$ N·m, the contour lines are sparser and sparser, causing the pressure moment coefficient to have opposite variation trend around the floating states with $M_P = 0.9 \times 10^8$ N·m and it is obviously shown in Figure 11b.

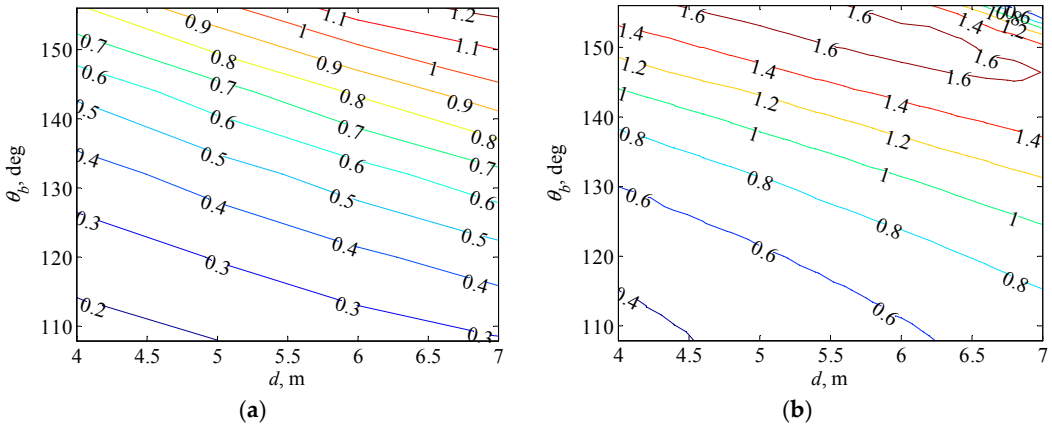

Figure 11. Pressure moment and pressure moment coefficient as a function of depth of rotation axis and beak angle: (**a**) pressure moment $M_P/10^8$ N·m; and (**b**) pressure moment coefficient $K_P/10^8$ N·m·rad^{-1}.

At equilibrium position, the Duck is balanced when the pressure moment equals the gravity moment as:

$$M_P - mgL\cos(\pi - \alpha) = 0 \tag{25}$$

where m is the rotating mass of the Duck. Then, the gravity moment coefficient can be deduced as:

$$K_G = \frac{\mathrm{d}(-mgL\cos(\pi - \alpha))}{\mathrm{d}\alpha} = -mgL\sin\alpha = M_P\tan\alpha \tag{26}$$

Hence, the gravity moment coefficient only depends on the pressure moment, i.e., the floating state, and the angle of gravity center of the rotating mass. In order for the Duck to be able to balance with the pressure moment, α should be between $\pi/2$ and $3\pi/2$. Thus, the gravity moment coefficient ranges from $-\infty$ to $+\infty$. That means it is possible to adjust the hydrostatic stiffness coefficient to any desired value so that Equation (17) be satisfied and complex conjugate control be realized to maximize power capture. Therefore, at different tidal heights, the variation of hydrodynamic coefficients can be followed by the adjustment of hydrostatic stiffness by changing the angle of mass center so that the reactance of the system impedance keep zero. Then, the WEC system will have the optimal performance in tide. Since the pressure moment coefficient increase with both depth of rotation axis and beak angle, the gravity moment coefficient will be more sensitive to the angle variance of gravity center of the rotating mass at large depth of rotation axis and beak angle.

4.4. Case Study

As a summation of the studies in above sections, we have firstly investigated the character of the hydrodynamic coefficients and maximum relative capture width of a solo Duck WEC at different floating states, and we make the complex conjugate control more credible by adjusting the beak angle to as large a value as possible so that the RAO will be reasonably small. Then, we proposed to realize the complex conjugate control by adjusting the angle of gravity center of the rotating mass of the Duck to cancel the reactance term of the mechanical impedance in different tidal heights. In this section, we apply the movable mass method to achieve complex conjugate control for a solo Duck WEC when exposed to tide by a case study.

For simplicity of engineering realization, the movable mass is better located inside the profile of the Duck. In this section, the movable mass is only free to move in the x-z plane as the movement in the y direction is meaningless to adjusting the hydrostatic stiffness coefficient and gravity moment. Supposing that the movable mass takes part of the total rotating mass, denoted as bm, where b is the mass ratio, and the movable mass is assumed to focus at one point to ease the calculation for its inertia. The designed floating state is selected as that listed in Table 2 when the tidal height is 0,

and the designed position of the movable mass is where the movable mass resides at the designed floating states. In order for the Duck to balance and resonate at the designed floating state, according to Equations (17), (25), and (26), it satisfies that:

$$M_d + (1-b)mgL_0\cos\alpha_0 + bmgL_d\cos\alpha_d = 0 \tag{27}$$

$$K_d - mg[(1-b)L_0\sin\alpha_0 + bL_d\sin\alpha_d] = (J_d + J_0 + bmL_d^2)\omega^2 \tag{28}$$

where M_d and K_d are the pressure moment and pressure moment coefficient at the designed floating state, respectively; L_d and α_d are the radial distance and angle of the designed position of the movable mass, respectively; J_d is the added inertia at the designed floating state; L_0 and α_0 are the radial distance and angle of the gravity center of remained rotating mass, respectively; and J_0 is the inertia of the remained rotating mass added with the converted inertia from the PTO load. At certain tidal height, in order for the Duck to balance and resonate at the corresponding floating state, it should satisfy that:

$$M_n + (1-b)mgL_0\cos(\alpha_0+\beta) + bmgL_n\cos(\alpha_n+\beta) = 0 \tag{29}$$

$$K_n - mg[(1-b)L_0\sin(\alpha_0+\beta) + bL_n\sin(\alpha_n+\beta)] = (J_n + J_0 + bmL_n^2)\omega^2 \tag{30}$$

where M_n and K_n are the pressure moment and pressure moment coefficient at this floating state, respectively; L_n and α_n are the radial distance and angle of the position of the movable mass at this floating state, respectively; J_n is the added inertia at this floating state; and β is the beak angle differences between this floating state and the designed floating state. From Equations (27)–(30), the following relations are derived:

$$M_n - M_d = -(1-b)mgL_0[\cos(\alpha_0+\beta) - \cos\alpha_0] - bmg[L_n\cos(\alpha_n+\beta) - L_d\cos\alpha_d] \tag{31}$$

$$\begin{aligned} &K_n - K_d - mg\{(1-b)L_0[\sin(\alpha_0+\beta) - \sin\alpha_0] + b[L_n\sin(\alpha_n+\beta) - L_d\sin\alpha_d]\} \\ &= [J_n - J_d + bm(L_n^2 - L_d^2)]\omega^2 \end{aligned} \tag{32}$$

To find the solution of α_n and L_n, Equations (31) and (32) can be rearranged as:

$$L_n = -\frac{M_n - M_d + (1-b)mgL_0[\cos(\alpha_0+\beta) - \cos\alpha_0] - bmgL_d\cos\alpha_d}{bmg\cos(\alpha_n+\beta)} \tag{33}$$

$$\begin{aligned} F_n =& K_n - K_d - mg\{(1-b)L_0[\sin(\alpha_0+\beta) - \sin\alpha_0] + b[L_n\sin(\alpha_n+\beta) - L_d\sin\alpha_d]\} \\ &-[J_n - J_d + bm(L_n^2 - L_d^2)]\omega^2 \end{aligned} \tag{34}$$

Then, α_n is traversed through all the value from $-\pi$ to π to find the corresponding L_n and F_n. One example of the variation of L_n and F_n with α_n is shown in Figure 12, where L_{lim} is the radial distance from the Duck surface to the rotation axis. Since the movable mass should be inside the Duck profile, the solution for L_n should be below the curve of L_{lim}. Then, the solution is found where F_n equals zero, and $0 < L_n < L_{\text{lim}}$. In all the calculations in this section, we assume the radial distance and angle of the remained rotating mass center to be constant, and they are set to L_0 = 2.5 m and $\alpha_0 = 135^\circ$.

Figure 13a shows the position of the movable mass variation with tidal height at different wave frequencies at L_d = 2.5 m, $\alpha_d = 135^\circ$ and b = 0.2. The movable mass finds its position inside Duck profile in the whole tidal range indicating that the movable mass method is able to make the Duck WEC work at resonance at every tidal height for different wave frequencies in the finite space inside the Duck profile. Figure 13b shows the position of the movable mass variation with tidal height at different mass ratios at L_d = 2.5 m, $\alpha_d = 135^\circ$ and f = 0.1 Hz. For the same variation of tidal height, the displacement of the movable mass decreases with mass ratio. At b = 0.3, the five positions of the movable mass corresponds to the five tidal heights listed in Table 2 are relatively compact. However, at b = 0.1, it is even not possible to find a place inside the Duck for the movable mass at tidal

height $d_T = -1.5$ m and $d_T = 1.5$ m to achieve resonance. Hence, the efficiency of the Duck in tidal range of 3 m will be reduced.

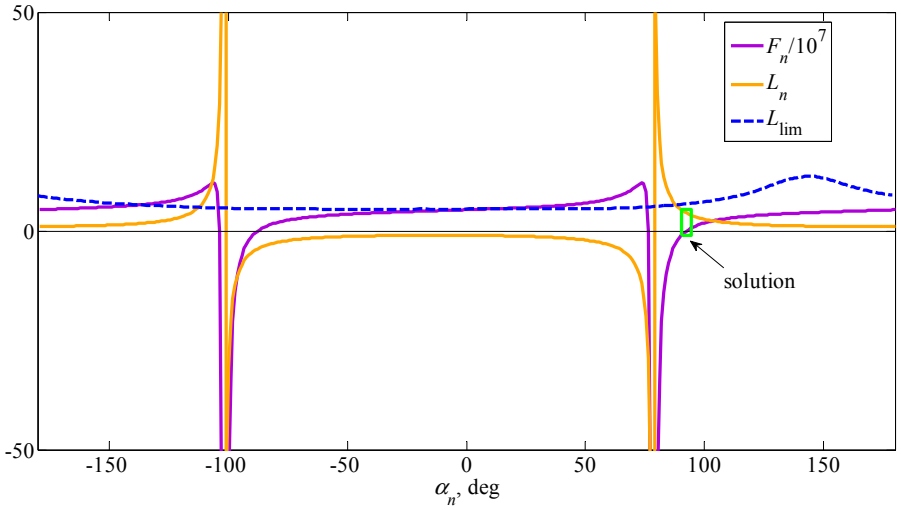

Figure 12. One example of the variation of L_n and F_n with α_n.

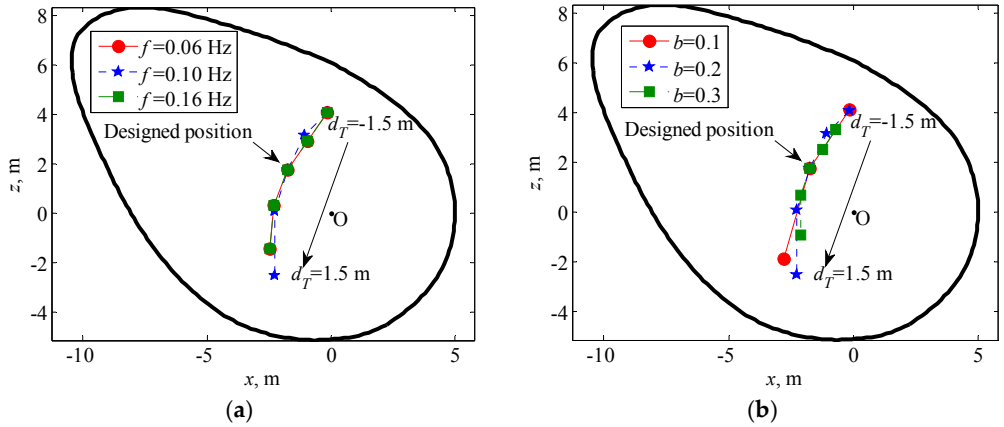

Figure 13. Position of the movable mass variation with tidal height at different wave frequencies and mass ratios: (**a**) for different wave frequencies at $L_d = 2.5$ m, $\alpha_d = 135°$, and $b = 0.2$; and (**b**) for different mass ratios at $L_d = 2.5$ m, $\alpha_d = 135°$, and $f = 0.1$ Hz.

Figure 14a shows the position of the movable mass variation with tidal height at different radial distance of the designed position at $\alpha_d = 135°$, $b = 0.2$, and $f = 0.1$ Hz. Slight increase in the displacement of the movable mass corresponding to the same tidal height variation for larger radial distance of the designed position has been observed. When approaching the beak part of the Duck, smaller room will be left for the movable mass to locate. At $L_d = 7.5$ m, there will be no position inside the Duck for the movable mass to locate to make the Duck WEC resonate when $d_T = -1.5$ m. Figure 14b shows the position of the movable mass variation with tidal height at different angles of the designed position at $L_d = 2.5$ m, $b = 0.2$, and $f = 0.1$ Hz. In addition, small increase in the displacement of the movable mass corresponding to the same tidal height variation for larger angle of the designed position is noticed. Nearer the boundary of the Duck profile of the designed position, smaller rooms will be left for the movable mass to locate. At $\alpha_d = 165°$, the movable mass is about to touch the boundary when $d_T = 1.5$ m. From the above analysis, the best designed position should be locate at the center of the Duck profile so that the displacement of the movable mass will be smaller and there will be enough room for the movable mass to locate for the whole tidal range.

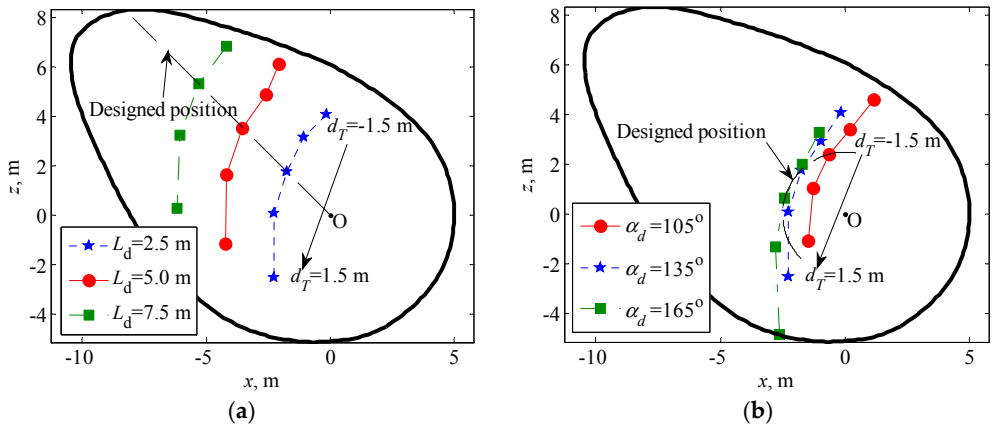

Figure 14. Position of the movable mass variation with tidal height at different wave frequencies and mass ratios: (**a**) for different radial distance of the designed position at α_d = 135°, b = 0.2, and f = 0.1 Hz; and (**b**) for different angle of the designed position at L_d = 2.5 m, b = 0.2, and f = 0.1 Hz.

From an engineering view, the heavier the movable mass, the more expensive the cost is. The weight of the movable mass can be calculated as:

$$G_m = bmg = \frac{M_d}{-L_0 \cos \alpha_0 \left(\frac{1}{b} - 1 + \frac{L_d \cos \alpha_d}{L_0 \cos \alpha_0} \right)} \tag{35}$$

As can be seen, the weight of the movable mass increases with mass ratio b, and decreases with L_d and cosα_d. In order to apply a light-weight movable mass, the mass ratio should be as small as possible, and a maximum value of $L_d$cosα_d inside the Duck profile suggests that the best designed position should reside on the paunch surface. However, the above studies find that the movable mass will not be able to stay inside the Duck in the whole tidal range if the mass ratio is too small and the designed position locates near the Duck profile boundary. Thus, to find the lowest weight, we should solve the optimization problem under constraints stated as below:

$$\begin{aligned} &\min \ G_m \\ &\text{subject to } L_n(\alpha_n) < L_{\text{lim}}(\alpha_n) \quad \text{for } d_T \in [-1.5,\ 1.5] \end{aligned} \tag{36}$$

From above studies, we found that the trajectory of the movable mass varies continuously with tidal height. Therefore, we believe that provided the position of the movable mass for the five tidal heights listed in Table 2 resides inside the Duck profile, the movable mass will always reside inside the Duck profile for the whole tidal range. Figure 15 shows the distribution of the lowest movable mass weight and corresponding mass ratio at different designed positions. In Figure 15a, the deep blue region represents the most suitable place for the designed position, and it resides at the center area of the Duck profile, which confirms the previous conclusion that the designed position should be kept away from the boundary. In Figure 15b, the mass ratio is smaller in the upper area of the Duck, while larger at the lower area. The blank area inside the Duck profile means that there will be no solution for Equations (29) and (30) at these regions. We found the minimum value of mass ratio to be 0.125 indicating that at least 12.5% of the rotating mass should be arranged to make the movable mass be adequate to realize complex conjugate control for the whole tidal range.

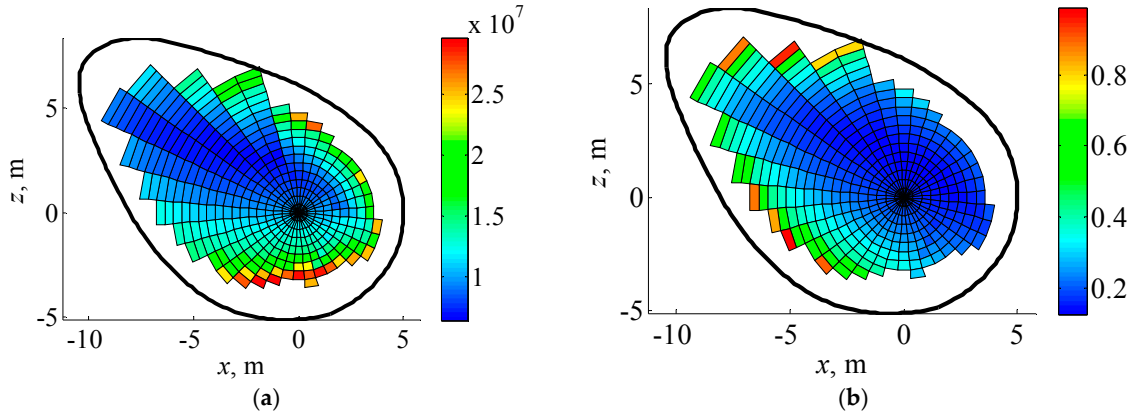

Figure 15. Distribution of the lowest movable mass weight and corresponding mass ratio at different designed positions: (**a**) lowest movable mass weight; and (**b**) corresponding mass ratio.

5. Conclusions

This paper studied the influence of tidal height to the hydrodynamic performance of a solo Duck wave energy converter with fixed pitching axis in regular wave. A movable mass method is utilized in the whole tidal range to not only balance the Duck to appropriate beak angle, but also follow the hydrodynamic coefficient variation to keep cancelling the reactance of the WEC system impedance so that complex conjugate control can be realized to optimize the Duck WEC performance in tide. Some conclusions can be made from above studies:

(1) The added inertia, radiation damping coefficient and excitation moment coefficient share similar variation law with floating states. Furthermore, the added inertia can be qualitatively estimated by the water inertia, which is defined as the mapped length on the Duck surface in the normal direction of its velocity multiplied by square of its rotation radius.

(2) In most of the range of the wave frequency investigated in this paper, the Duck WEC has a maximum relative capture width larger than one, which is consistent with the point absorber effect. The beak angle should be adjusted to as large a value as possible so that the RAO of the Duck at maximum relative capture width will be reasonably small.

(3) At certain floating state, the hydrostatic stiffness coefficient only depends on the angle of mass center. Therefore, the position of the mass center is a key parameter that not only balances the Duck to a large beak angle, but also adjusts the reactance of the system so that complex conjugate control can be realized at different tidal heights.

(4) In order to cancel the reactance term from the mechanical impedance of the WEC system at different tidal heights, the movable mass ratio should not be too small, and the designed position of the movable mass should keep away from the Duck profile. The lowest weight of the movable mass is found when its designed position locates at the center of the Duck profile.

Acknowledgments: The research was supported by the Chinese Scholarship Council (CSC) and the Swedish Research Council (VR) Grant 2015-04657.

Author Contributions: Jinming Wu performed the numerical simulation and prepared the manuscript. Yingxue Yao and Malin Göteman supervised the wave power project, commented on the manuscript and contributed to the revisions. Wei Li and Liang Zhou commented on the manuscript.

Conflicts of Interest: The authors declare no conflict of interest.

Nomenclature

A_0	Amplitude of the incident wave (m)
A^+	Radiated wave amplitude at $x \to +\infty$ due to forced unit amplitude pitching velocity (m)
A^-	Radiated wave amplitude at $x \to -\infty$ due to forced unit amplitude pitching velocity (m)
$\hat{A}$	Complex amplitude of wave amplitude (m)
b	Mass ratio
C	Radiation damping coefficient in pitch direction due to pitch motion (N·m·s)
C_e	PTO damping coefficient (N·m·s)
d	Depth of rotation axis (m)
ds	Length of the segment on the Duck surface (m)
d_T	Tidal height (m)
$E_{\max}$	Maximum efficiency
G	Gravity center of the rotating mass
G_m	Weight of the movable mass (N)
g	Acceleration of gravity (m/s^2)
h	Water depth (m)
J	Added inertia in pitch direction due to pitch motion (Kg·m^2)
J_0	Inertia of the remained rotating mass added with the converted inertia from the PTO load (Kg·m^2)
J_d	Added inertia at the designed floating state (Kg·m^2)
J_e	Dry inertia in pitch direction (Kg·m^2)
J_n	Added inertia at current floating state (Kg·m^2)
J_w	Water inertia (m^3)
K_d	Pressure moment coefficient at the designed floating state (N·m)
K_G	Gravity moment coefficient (N·m)
K_n	Pressure moment coefficient at this floating state (N·m)
K_P	Pressure moment coefficient (N·m)
K_r	Hydrostatic stiffness coefficient in pitch direction due to pitch motion (N·m)
k	Wave number
L	Radial distance of the gravity center of the rotating mass (m)
L_0	Radial distance of the gravity center of remained rotating mass (m)
L_d	Radial distance of the designed position of the movable mass (m)
$L_{\lim}$	Radial distance from the Duck surface to the rotation axis (m)
L_n	Radial distance of the position of the movable mass at current floating state (m)
l	Rotation radius of the small segment on the Duck surface (m)
M_0	Modulus of complex amplitude of excitation moment per unit wave amplitude (N)
M_d	Pressure moment at the designed floating state (N·m)
M_G	Gravity moment (N·m)
M_n	Pressure moment at this floating state (N·m)
M_P	Pressure moment (N·m)
$\hat{M}$	Complex amplitude of excitation moment in pitch direction (N·m)
n	Outward normal vector on the wetted surface
n_3	z-component of the normal vector n
O	Rotation axis
R	Radius of the stern part (m)
r	Vector from the point on the wetted surface to the rotation axis O
v	Volume of water displaced by the Duck (m^3)
W	Width of the Duck (m)
x	Component of a Cartesian coordinate system in wave propagating direction
y	Component of a Cartesian coordinate system in longitudinal direction of the Duck
Z	Radiation impedance (N·m·s)
Z_s	Mechanical impedance (N·m·s)
z	Component of a Cartesian coordinate system in the opposite direction of gravity
z_b	z-component coordinate of buoyancy center (m)
α	Angle of the gravity center of rotating mass (°)
α_d	Angle of the designed position of the movable mass (°)

α_0 Angle of the gravity center of remained rotating mass (°)
α_n Angle of the position of the movable mass at this floating state (°)
β Beak angle differences between this floating state and the designed floating state (°)
γ Angle between the normal vector of the segment and its velocity direction (°)
η Relative capture width
η_{max} Maximum relative capture width
θ Direction angle of the incident wave (°)
θ_b Beak angle (°)
ξ Pitch excursion (rad)
ξ_0 Modulus of complex amplitude of pitch excursion per unit wave amplitude (rad/m)
ξ_{0max} RAO of the solo Duck at the maximum relative capture width (rad/m)
$\hat{\xi}$ Complex amplitude of pitch excursion (rad)
$\dot{\hat{\xi}}$ Complex amplitude of pitch velocity (rad/s)
$\ddot{\hat{\xi}}$ Complex amplitude of pitch excursion (rad/s^2)
ρ Density of water (kg/m^3)
ϕ Phase difference between the complex amplitude of pitch excursion and $\hat{A}$ (°)
ω Circular frequency of incident wave (rad/s)

References

1. Vicinanza, D.; Margheritini, L.; Kofoed, J.P.; Buccino, M. The SSG wave energy converter: Performance, status and recent developments. *Energies* **2012**, *5*, 193–226. [CrossRef]
2. Iuppa, C.; Contestabile, P.; Cavallaro, L.; Foti, E.; Vicinanza, D. Hydraulic performance of an innovative breakwater for overtopping wave energy conversion. *Sustainability* **2016**, *8*, 1226. [CrossRef]
3. Hansen, R.H.; Kramer, M.M.; Vidal, E. Discrete displacement hydraulic power take-off system for the Wavestar wave energy converter. *Energies* **2013**, *6*, 4001–4044. [CrossRef]
4. Salter, S.H. Wave power. *Nature* **1974**, *249*, 720–724. [CrossRef]
5. Skyner, D. *Solo Duck Linear Analysis*; University of Edinburgh: Edinburgh, UK, 1987.
6. Salter, S.H. Apparatus and Method for Extracting Wave Energy. U.S. Patent 3,928,967, 30 December 1975.
7. Evans, D.V. A theory for wave-power absorption by oscillating bodies. *J. Fluid Mech.* **1976**, *77*, 1–25. [CrossRef]
8. Mei, C.C. Power extraction from water waves. *J. Ship Res.* **1976**, *20*, 63–66.
9. Cruz, J. *Ocean Wave Energy Current Status and Future Perspectives*; Springer: Berlin, Germany, 2008.
10. Pizer, D. *Numerical Modeling of Wave Energy Absorbers*; University of Edinburgh: Edinburgh, UK, 1994.
11. Mynett, A.E.; Serman, D.D.; Mei, C.C. Characteristics of Salter's cam for extracting energy from ocean waves. *Appl. Ocean Res.* **1979**, *1*, 13–20. [CrossRef]
12. Castellucci, V.; Garcia-Teran, J.; Eriksson, M.; Padman, L.; Waters, R. Influence of sea state and tidal height on wave power absorption. *IEEE J. Ocean. Eng.* **2016**, *PP*, 1–8. [CrossRef]
13. Castellucci, V.; Abrahamsson, J.; Kamf, T.; Waters, R. Nearshore tests of the tidal compensation system for point-absorbing wave energy converter. *Energies* **2015**, *8*, 3272–3291. [CrossRef]
14. Castellucci, V.; Waters, R.; Eriksson, M.; Leijon, M. Tidal effect compensation system for point absorbing wave energy converters. *Renew. Energy* **2013**, *51*, 247–251. [CrossRef]
15. Lucas, J.; Salter, S.H.; Cruz, J.; Taylor, J.R.M.; Bryden, I. Performance optimization of a modified Duck through optimal mass distribution. In Proceedings of the 8th European Wave and Tidal Energy Conference, Uppsala, Sweden, 7–9 September 2009.
16. Park, Y.H.; Suh, K.D. Variations of storm surge caused by shallow water depths and extreme tidal ranges. *Ocean Eng.* **2012**, *55*, 44–51. [CrossRef]
17. Khan, D.; Watson, S.J.; Infield, D.G. Identifying the effect of tidal height on offshore wind speed profiles. *Wind Energy* **2003**, *6*, 405–412. [CrossRef]
18. Masselink, G.; Short, A.D. The effect of tidal range on beach morphodynamics and morphology: A conceptual beach model. *J. Coast. Res.* **1993**, *9*, 785–800.
19. Falnes, J. *Ocean Waves and Oscillating Systems: Linear Interaction including Wave-Energy Extraction*; Cambridge University Press: Cambridge, UK, 2002.

20. Li, Y.; Yu, Y.H. A synthesis of numerical methods for modeling wave energy converter-point absorbers. *Renew. Sustain. Energy Rev.* **2012**, *16*, 4352–4364. [CrossRef]
21. McCormick, M.E. *Ocean Wave Energy Conversion*; Dover Publications Inc.: New York, NY, USA, 2007.
22. Price, A.A.E.; Dent, C.J.; Wallace, A.R. On the capture width of wave energy converters. *Appl. Ocean Res.* **2009**, *31*, 251–259. [CrossRef]
23. Lopes, M.F.P.; Hals, J.; Gomes, R.P.F.; Moan, T.; Gato, L.M.C.; Falcão, A. Experimental and numerical investigation of non-predictive phase-control strategies for a point-absorbing wave energy converter. *Ocean Eng.* **2009**, *36*, 386–402. [CrossRef]
24. Kara, F. Time domain prediction of power absorption from ocean waves with wave energy converter arrays. *Renew. Energy* **2016**, *92*, 30–46. [CrossRef]
25. Ansys, Inc. *AQWA Reference Manual*, version 16.0; Ansys, Inc.: Canonsburg, PA, USA, 2015.
26. Salter, S.H. Progress on Edinburgh ducks. In Proceedings of the IUTAM Symposium on Hydrodynamics of Ocean Wave Energy Utilization, Lisbon, Portugal, 8–11 July 1985.
27. Pizer, D. Numerical prediction of the performance of a solo Duck. In Proceedings of the 1993 European Wave Energy Symposium, Edinburgh, UK, 21–24 July 1993; pp. 129–137.
28. Evans, D.V. Maximum wave-power absorption under motion constraints. *Appl. Ocean Res.* **1981**, *3*, 200–203. [CrossRef]
29. Pizer, D.J. Maximum wave-power absorption of point absorbers under motion constraints. *Appl. Ocean Res.* **1993**, *15*, 227–234. [CrossRef]
30. Hals, J.; Falnes, J.; Moan, T. Constrained Optimal Control of a Heaving Buoy Wave-Energy Converter. *J. Offshore Mech. Arct. Eng.* **2010**, *133*, 011401. [CrossRef]
31. Newman, J.N. *Marin Hydrodynamics*; Massachusetts Institute of Technology (MIT) Press: Cambridge, MA, USA, 1977.